ACS Catalysis

Research Article

pubs.acs.org/acscatalysis

Influence of Weak Brønsted Acids on Electrocatalytic CO_2 Reduction by Manganese and Rhenium Bipyridine Catalysts

Christoph Riplinger[†] and Emily A. Carter*[,†,‡,⊥]

[†]Department of Mechanical and Aerospace Engineering, [‡]Program in Applied and Computational Mathematics, and [⊥]Andlinger Center for Energy and the Environment, Princeton University, Princeton, New Jersey 08544-5263, United States

Supporting Information

ABSTRACT: $[Re(bpy)(CO)_3]^-$ and $[Mn(bpy)(CO)_3]^-$ are homogeneous electrocatalysts for the reduction of CO_2 to CO. Their turnover frequencies depend on the type of Brønsted acid used, with the Mn catalyst exhibiting no catalytic turnover without added Brønsted acid. In this work, we use density functional theory together with continuum solvation and microkinetics simulations to understand these differences. The computed turnover frequencies reproduce the experimental trends. In absolute numbers, the computed turnover frequencies differ from the experimental ones by about an order of magnitude. We find that some of the experimentally used acids are too weak to protonate CO_2 or to stabilize CO_2 binding. Catalysis with these acids requires more negative applied potentials or higher acid concentrations compared to catalysis with stronger acids. This trend is more pronounced for the Mn catalyst than for the Re catalyst, the latter working at maximum turnover with acids that produce submaximum turnover with the Mn catalyst. In the absence of Brønsted acids, the first catalytic steps are driven by the solvent acetonitrile, which can act as proton donor for protonation of CO_2 in the case of the Re catalyst. For the Mn catalyst, the endergonic CO_2 binding free energy prevents protonation by acetonitrile. C−O bond cleavage, however, cannot be assisted by acetonitrile for either catalyst. Electrolyte-assisted C−O bond cleavage via Hofmann degradation is also predicted to be strongly disfavored kinetically. Water produced during catalysis might be responsible for completing the reaction cycle.

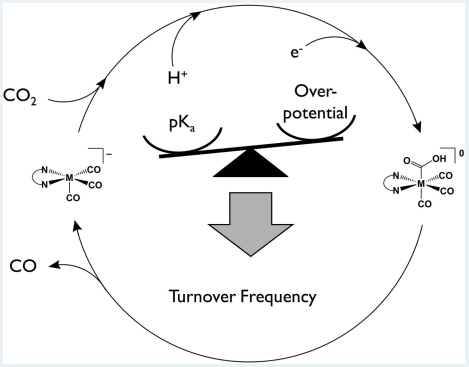

KEYWORDS: *CO_2 reduction, Brønsted acid, electrocatalysis, homogeneous catalysis, turnover frequencies, microkinetics simulation*

INTRODUCTION

Emerging renewable energy production will decrease our dependence on fossil fuels; however, the supply of renewable energy sources fluctuates, a serious drawback. To serve demands in times of low supply, excess electricity at high supply times has to be stored for later use. One promising avenue for energy storage is to convert electricity into chemical energy, which then can be converted back in times of low renewable electricity production. Reducing CO_2 to energetically richer molecules, such as CO, methanol, or longer-chain alcohols, is one possible means to store energy, having the additional advantage of closing the carbon cycle.[1,2]

CO_2 reduction catalysts have been investigated over the last four decades,[3−12] and it is now widely accepted that the homogeneous *fac*-Re(bpy-R)$(CO)_3$Cl (bpy-R = 4,4′-disubstituted-2,2′-bipyridine) electrocatalysts are superior to many others in terms of rates, selectivities, and lifetimes.[13−16] Their properties have been extensively investigated on an experimental and to some extent a computational level.[13−27] In 2011, it was shown that the much more abundant Mn can be used as a substitute for Re, yielding the Mn(bpy-R)$(CO)_3$Br complexes. These complexes exhibit properties similar to the Re catalysts and reduce CO_2 at an even lower overpotential.[18,28] Both the Mn and Re catalysts operate in organic solvents (e.g., acetonitrile, MeCN), are highly selective towards CO_2 to CO reduction, and involve the doubly reduced $[M(bpy-R)(CO)_3]^-$ (M = Mn or Re) as the active catalyst.

Recently, we compared the mechanisms of the Mn(bpy)$(CO)_3$Br and the Re(bpy)$(CO)_3$Cl catalysts using quantum chemistry combined with continuum solvation and microkinetics.[25] The investigated CO_2 reduction cycle is depicted in Figure 1. The active catalyst **3** initially binds CO_2 (**3** → **5**), which immediately gets protonated (**5** → **6**). From **6**, two different pathways can be taken. In the reduction-first pathway, **6** gets reduced to **8** before the C−O bond is cleaved. In the protonation-first pathway, the C−O bond is cleaved first (**6** → **7**) and then **7** gets further reduced. Both pathways end up in species **2** (the Mn complex, **2-Mn**, spontaneously loses the produced CO ligand) or **2CO** (the produced CO ligand stays bound to the Re complex, **2CO-Re**). From **2-Mn**/**2CO-Re**, a second reduction takes place, **2CO-Re** loses its CO ligand, and the active catalyst is regenerated. Our results showed that the Mn complex has a lower binding affinity to a sixth ligand, resulting in a stronger tendency to dimerize than the Re

Received: October 30, 2014
Revised: December 19, 2014
Published: December 22, 2014

DOI: 10.1021/cs501687n
ACS Catal. 2015, 5, 900−908

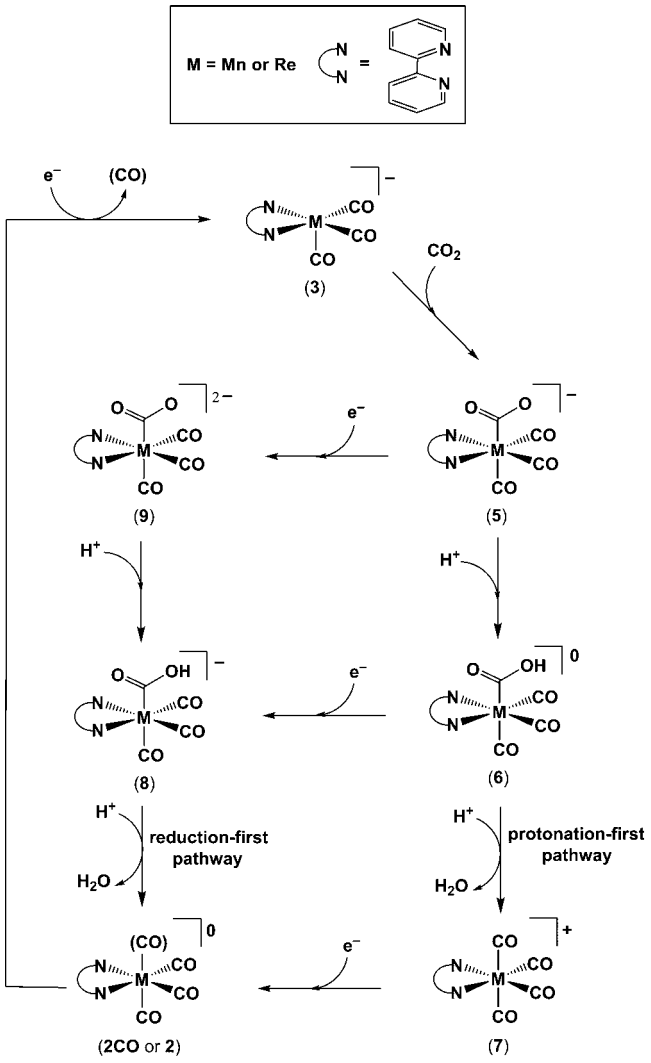

Figure 1. CO_2 reduction catalytic cycle for the $[Mn(bpy)(CO)_3]^-$ and $[Re(bpy)(CO)_3]^-$ active catalysts, using the same nomenclature as in ref 25. Note that, compared with ref 25, species **9** is added to the cycle.

catalyst. Also, for the Mn catalyst, protonation of **5** is necessary to stabilize binding of the CO_2 ligand, as CO_2 binding alone is endergonic. The benefit of its lower sixth ligand binding affinity is that the Mn catalyst exhibits a lower overpotential. This results in the flexibility to traverse both pathways. The Mn catalyst can access the protonation-first pathway at applied potentials between −1.4 and −1.7 V vs SCE, and the reduction-first pathway at more negative potentials. The Re catalyst, on the other hand, operates at higher overpotential only and thus is restricted to the reduction-first pathway.

CO_2 reduction by the Re and Mn catalysts is dependent on cosubstrates that provide protons. Wong et al. investigated the effect of various weak Brønsted acids on electrocatalytic CO_2 reduction by $[Re(bpy)(CO)_3(py)]^+$.[16] They examined reactions with four acids: 2,2,2-trifluoroethanol (TFE), phenol, methanol (MeOH), and water (H_2O). They found that the efficiency of the catalyst increases with the acidity of the Brønsted acid used. Phenol and TFE, the strongest acids, exhibit the largest efficiency while catalysis with MeOH is two orders of magnitude slower, and H_2O is one order of magnitude slower than with MeOH. The authors point out that for phenol and TFE, the acid concentration at which maximum turnover frequency (TOF) is achieved is about 10 to 20 times lower than for MeOH and H_2O. Bourrez et al. showed that $[Mn(bpy)(CO)_3Br]$ electrocatalyzes CO_2 if H_2O is present but not noticeably without.[28] In our previous work, we showed that the same catalyst with phenol shows a TOF about three to four orders of magnitude higher than with H_2O.[25]

Smieja et al. investigated the influence of different Brønsted acids on CO_2 electrocatalytic reduction by $[Mn(bpy\text{-}tBu)(CO)_3Br]$ and compared their results with previous ones for the Re catalyst.[14,18] They found that with H_2O as the Brønsted acid, the Mn catalyst is faster than the Re catalyst. With all other acids, both catalysts exhibit similar TOFs. The authors report that the room temperature rate constant of the Re catalyst decreases in the order TFE > MeOH > H_2O (410, 94, and 5.7 s^{-1}), whereas the trend for the Mn catalyst is TFE > MeOH ≈ H_2O (340, 130, and 120 s^{-1}). An interesting difference between the Re and Mn catalysts is that the Re catalyst also operates without an external H^+ source, albeit at very low TOFs.[18] This is not the case for the Mn catalyst, which requires the addition of weak Brønsted acids to be able to react with CO_2 and thus to exhibit catalytic turnover in electrocatalysis.[18]

In this work, we investigate the influence of different Brønsted acids and applied potentials on electrolytic CO_2 reduction catalyzed by both the Re and Mn complexes. Hybrid density functional theory (DFT) + continuum solvation calculations are employed for structural optimization of reaction intermediates and transition states, in particular for the rate-limiting steps involving different Brønsted acids as cosubstrates. We perform microkinetics simulations of the catalytic reaction course using new cosubstrates. Reduction potentials, reaction free energies, and activation barriers for these simulations are partly taken from ref 25 and partly obtained in this work in the case of new reaction steps. The microkinetics simulations help us to understand the effect of the different Brønsted acids on the catalytic cycle and on the catalytic turnover.

METHODS

All quantum chemical calculations were performed using the ORCA program package.[29] In this work, we apply the same methodologies as in ref 25. In the previous work, only phenol was used as the proton donor for the barrier calculations. In this study, the set of proton donors is extended to include the ones used experimentally—namely, the Brønsted acids TFE, H_2O, and MeOH—as well as the solvent molecule MeCN and the cation tetrabutylammonium (TBA) of the electrolyte tetrabutylammonium hexafluorophosphate, two other potential proton sources when no Brønsted acids are present. During the study, it turned out that including these new Brønsted acids in the calculation caused new challenges. The structure optimization protocol had to be modified for the weaker acids. Also, the microkinetics simulation script was adapted to incorporate new pathways.

Computational Methodology. Because transition state (TS) optimizations in the gas phase did not converge for the acids TFE, MeOH, H_2O, and for MeCN and TBA applying the original methodology, it was necessary to change the protocol for some specific calculations. Geometry optimizations for all structures involving these species instead always employ the conductor-like screening model (COSMO) simulating the solvent MeCN as a dielectric continuum (ε = 36.6, refractive

DOI: 10.1021/cs501687n
ACS Catal. 2015, 5, 900−908

index = 1.334)[30] and are not optimized in the gas phase as well, as was possible for phenol in our earlier work. For these new calculations, the minimally augmented def2-SVP basis set,[31] together with an appropriate auxiliary basis (automatically generated by ORCA), is applied instead of the respective basis set without diffuse functions.

Our methodology is different than in ref 25, where we used the explicit solvation energy of a proton in MeCN (−260.2 kcal/mol)[20,32] for each added proton. In this work, protonation steps explicitly incorporate the proton donor

$$A^- + BH \leftrightarrow AH + B^- \quad (1)$$

with the Brønsted acid/base pair BH/B^- and the species A^- that gets protonated. As described in the Supporting Information (SI), the acid/base pairs are solvated explicitly by MeCN molecules. The respective Brønsted acid or MeCN or TBA is used to calculate the barrier for C−O bond cleavage, which is the rate-limiting step of the catalytic cycle.

Microkinetics Simulations and Activation Barriers. In ref 25, protonation steps were thermodynamically highly favorable and thus were considered to run to completion. This is not the case when using explicit Bronsted acids; those steps now have to be treated differently, including forward as well as backward reactions. The microkinetics script used in the previous work was modified accordingly. The barriers for the backward reactions were computed as

$$\Delta G^{\neq,\circ}_{\leftarrow} = \Delta G^{\neq,\circ}_{\rightarrow} - \Delta G^{\circ} \quad (2)$$

where $\Delta G^{\neq,\circ}_{\leftarrow}$ and $\Delta G^{\neq,\circ}_{\rightarrow}$ are the activation barriers for backward and forward reactions, respectively, and ΔG° is the reaction free energy for the reaction (all obtained at the standard state of 1 M, 298.15 K, and 1 atm for all species). If barriers become too small, the microkinetics simulation becomes unstable. In those cases, an equal shift is applied to both barriers to produce a minimum barrier height of 1 kcal/mol as well as maintaining the relation in eq 2.

In ref 25, the activation barriers for the rate-limiting steps were calculated at two levels of theory. Single-point energies were calculated at the DFT-B3LYP[33−35] plus dispersion correction[36] level as well as at the LPNO−CCSD[37] level. The computed TOFs from the microkinetics simulations were several orders of magnitude too high when using the DFT barriers and were greatly improved upon using the coupled-cluster barriers. Using the CCSD barriers corresponds to a positive shift of the DFT barriers of 2.4 and 2.9 kcal/mol for the protonation-first and reduction-first pathway, respectively, with the Re catalyst, and of 4.7 kcal/mol for both barriers with the Mn catalyst. In this work, we calculate the barriers at the DFT-B3LYP level only. To refine the barriers, shifts similar to the ones in ref 25 are applied. It is reasonable to assume that the shift is specific to the catalyst. Thus, the shift is calculated as the average of the two shifts that were obtained for each catalyst, 2.65 kcal/mol for the Re catalyst and 4.7 kcal/mol for the Mn catalyst.

As in ref 25, bimolecular rate constants were computed using classical transition state theory,[38,39] calculated as

$$k = \frac{k_B \cdot T}{h} \cdot K^{\circ} \cdot \exp\left(\frac{-\Delta G^{\neq,\circ}}{R \cdot T}\right) \quad (3)$$

where k is the rate constant, k_B is the Boltzmann constant, T is the temperature, h is Planck's constant, K° is the inverse of the standard state concentration (1 M), R is the universal gas constant, and $\Delta G^{\neq,\circ}$ is the standard free energy of activation (obtained at the standard state of 1 M, 298.15 K, and 1 atm for all species).

The initial microkinetics simulation conditions were chosen as in ref 25; namely, 1 mM catalyst concentration, 0.3 M CO_2 concentration (concentration of saturated CO_2 in MeCN),[16] 0.57 M acid with the Re complex, and 0.21 M acid with the Mn complex.

RESULTS AND DISCUSSION

Effect of Brønsted Acid pK_a on the Applied Potential for CO_2 Reduction. Before investigating the effect of the choice of Brønsted acid on electrocatalytic CO_2 reduction, we first study the effect of the acidity on the overall thermodynamics of CO_2 reduction in acetonitrile. The net equation for CO_2 reduction to CO is

$$CO_2 + 2H^+ + 2e^- \leftrightarrow CO + H_2O \quad (4)$$

The free energy of this reaction can be computed using the free energy of a free electron in MeCN, which depends on the applied potential, and the pK_a of the proton source in MeCN (see eq 9 in the SI). Because electrocatalytic CO_2 reduction happens under constant CO_2 influx and excess CO constantly bubbles out of the solution, we assume that the concentrations of CO_2 and CO are the saturated concentrations of CO_2 and CO in acetonitrile (300 mM and 8 mM, respectively).[16,35] The result is displayed in Figure 2. The plotted line shows the applied potential at which ΔG° = 0 kcal/mol for reaction 4, depending on the pK_a of the proton donor. For all applied potential/pK_a combinations below this line, the equilibrium of reaction 3 lies on the right side, that is, CO_2 is reduced to CO, and for all combinations above this line, the equilibrium lies on the left side, that is, CO_2 is not reduced. This idealized and

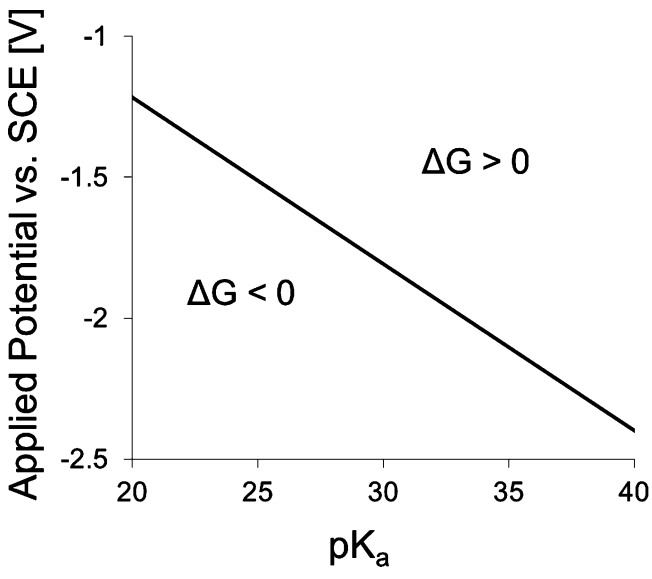

Figure 2. Applied potential/pK_a diagram mapping endergonic and exergonic regions for electrochemical CO_2 reduction in acetonitrile ($CO_2 + 2H^+ + 2e^- \leftrightarrow CO + H_2O$). The applied potential (in V vs SCE) and the pK_a determine the free energy of the reducing electrons and the protons. The solid line indicates where ΔG = 0. All values are given for standard states at room temperature, with the exception of the CO_2 and CO concentrations. CO_2 and CO concentrations are assumed to be 300 and 8 mM, respectively (corresponding to the concentration of saturated CO_2 and saturated CO in acetonitrile).[16,40]

DOI: 10.1021/cs501687n
ACS Catal. 2015, 5, 900−908

simple model, compared with actual CO_2 electrocatalytic reduction, neglects any sources for overpotential. However, it gives us an upper bound, defining a theoretical minimum applied potential for a given pK_a.

The computed pK_a values of the Brønsted acids used in this work are summarized in Table 1, covering a range between 21

Table 1. Computed pK_a Values in Acetonitrile of the Brønsted Acids Used in This Study[a]

Brønsted acid	computed pK_a in acetonitrile
phenol	21.6
TFE	26.4
H_2O[b]	30.7
H_2O[c]	26.6
MeOH	30.5

[a]The pK_a values are computed for explicitly solvated acid/base pairs (see the SI). All values, except where noted, are given for standard states at room temperature. [b]H_2O in acetonitrile without CO_2. [c]H_2O in acetonitrile with a 0.3 M CO_2 concentration (saturated CO_2 in MeCN)[16]

and 31. H_2O in the presence of CO_2 acidifies by forming carbonic acid ($H_2O + CO_2 \leftrightarrow H_2CO_3$). Because all experiments and simulations for CO_2 reduction with H_2O as Brønsted acid use an acetonitrile solution saturated with CO_2, we compute the pK_a of H_2O in equilibrium with carbonic acid ($H_2O + CO_2 \leftrightarrow H_2CO_3 \leftrightarrow H^+ + HCO_3^-$). It can be seen from Figure 2 that when phenol is used, a theoretical minimum applied potential of about −1.3 V vs SCE is necessary to drive CO_2 reduction forward, a potential significantly less negative than necessary when using the Re catalyst (−1.7 V vs SCE).[25] For the weaker Brønsted acid MeOH, a much more negative applied potential of −1.8 V vs SCE is necessary, a potential at which the Mn and Re catalysts prefer to take the reduction-first pathway. This simple model already predicts that when using weak Brønsted acids, (i) a potential of about −1.8 V vs SCE or more negative has to be applied and (ii) the reaction proceeds preferentially via the reduction-first pathway using the Re and Mn catalysts.

Effect of Brønsted Acids on CO_2 Binding. Previously, we reported that the observed differences in Brønsted acid dependence between the Re and the Mn catalyst can be rationalized by their differences in CO_2 binding.[25] Binding of CO_2 to Re is exergonic (−3.4 kcal/mol) and to Mn is endergonic (2.2 kcal/mol). Only subsequent protonation, using an available proton, drives the reaction forward and stabilizes CO_2 binding to Mn, resulting in species **6** or (further reduced) species **8**. Species **6** and **8** are the reactants of the rate-limiting C−O bond cleavage steps and thus their stability is crucial for catalytic turnover. The model in ref 25 uses a phenol molecule as an explicit proton donor. Phenol, in turn, gets protonated by a solvated proton in acetonitrile. In this work, we use a more refined protonation model. The only proton source in this model is a Brønsted acid, and there is no bath of solvated protons in acetonitrile available. This refined model allows us to investigate the influence of different Brønsted acids on CO_2 binding. The pK_a values of the Brønsted acids given in Table 1 already indicate that protonation will be much less exergonic compared with the model in ref 25 because a free solvated proton in acetonitrile has a pK_a value of 0. Table 2 summarizes the reaction free energies for CO_2 binding to the active catalyst **3** and protonation of the CO_2 adduct **5**. With the previous

Table 2. Overall Reaction Free Energies (kcal/mol) for Protonation of 5-Mn and 5-Re (5 → 6) As Well As for CO_2 Binding to the Active Catalysts 3-Mn and 3-Re and Subsequent Protonation (3 → 6) for Different Brønsted Acids[a]

	ΔG (5 → 6)		ΔG (3 → 6)	
proton source	Mn catalyst	Re catalyst	Mn catalyst	Re catalyst
H^+ in MeCN	−33.4	−34.0	−31.1	−37.4
phenol	−3.9	−4.5	−1.6	−8.0
TFE	2.6	2.0	4.9	−1.5
H_2O[b]	2.9	2.3	5.2	−1.1
MeOH	8.2	7.6	10.5	4.1

[a]All values are given for standard states at room temperature. [b]H_2O in acetonitrile with a 0.3 M CO_2 concentration (saturated CO_2 in MeCN).[16]

protonation scheme (H^+ in MeCN in Table 2), **5** → **6** and thus **3** → **6** are highly exergonic. With the refined protonation scheme, **5** → **6** is endergonic for both catalysts using TFE, MeOH, and H_2O. For the Mn catalyst, these energetics imply that **3-Mn** will be the most stable intermediate, whereas for the Re catalyst, CO_2-bound **5-Re** is the most stable. For both catalysts, only protonation with phenol is exergonic and drives the reaction forward to stabilize **6**. Because CO_2 binding is crucial for the next reaction steps and catalytic turnover (vide supra), we investigate potential new scenarios for CO_2 binding in the next paragraph.

Stabilization of CO_2 Binding. In the previous reaction mechanism from ref 25, species **5** is directly protonated to **6** and subsequently reduced to **8** (or alternatively, the C−O bond of **6** is cleaved, **6** → **7**). Here we expand the reaction model to allow for the reverse ordering of protonation and reduction steps, that is, we also consider reduction of **5** to **9**, and subsequent protonation to yield **8**, introducing the reduced CO_2-bound species **9**. The extended reaction mechanism considered in this work is summarized in Figure 1. It should be noted that proton-coupled CO_2 binding can also be simulated. This might influence the barrier for CO_2 binding; however, because (i) the barriers for CO_2 addition are very low compared to the other barriers in the reaction cycle and (ii) the overall thermodynamics of CO_2 addition is not influenced by simultaneous or consecutive CO_2 binding and protonation, we assume that CO_2 binding and protonation occur consecutively.

As expected from the differences in net charges (−2 for **9** and −1 for **5**), the proton affinity of **9** is found to be much higher than that of **5** (Table 3). Indeed, these data reveal that protonation of **9** is favorable for phenol, TFE, and H_2O and thermoneutral for MeOH. However, of course the reduction potential is also influenced by differences in charge on the complex (Table 4). The reduction potential of **5** is computed to be −1.87 and −2.03 V vs SCE for Re and Mn, respectively. These reduction potentials are ∼0.3 V more negative than those of **6** (with a net charge of 0 for **6** and −1 for **5**). This means that the higher proton affinity of **9** is balanced out by the higher potential that has to be applied to reduce **5** to **9**.

We also calculated the reduction potential of **9**. This is ∼0.5 V more negative than the reduction potential of **5**, which shows that, at the experimentally applied potentials, protonation is necessary before the next reduction can take place.

To compare the reaction pathways before C−O bond cleavage, it is instructive to visualize the free energy changes

DOI: 10.1021/cs501687n
ACS Catal. 2015, 5, 900−908

Table 3. Overall Reaction Free Energies (kcal/mol) for Protonation of 9-Mn and 9-Re (9 → 8) for Different Brønsted Acids[a]

	ΔG (9 → 8)	
proton source	Mn catalyst	Re catalyst
H^+ in MeCN	−41.2	−41.1
phenol	−11.7	−11.6
TFE	−5.2	−5.1
H_2O[b]	−5.6	−5.5
MeOH	0.4	0.5

[a]All values are given for standard states at room temperature. [b]H_2O in acetonitrile with a 0.3 M CO_2 concentration (saturated CO_2 in MeCN).[16]

Table 4. Computed One-Electron Reduction Potentials (V vs SCE) for the Reduction Steps before C−O Bond Cleavage in the Mn and Re Catalytic Cycle[a]

reduction	potential (Mn catalyst)	potential (Re catalyst)
6 → **8**	− 1.69[b]	− 1.56[b]
5 → **9**	− 2.03	− 1.87
reducing **9**	− 2.50	− 2.31

[a]See Figure 1. All values are given for standard states at room temperature. [b]From ref 25.

during reaction with one of the Brønsted acids. Figure 3 shows these data for both catalysts with H_2O as the proton source at −2.03 and −1.87 V vs SCE, respectively, for Mn and Re (the minimum applied potentials at which **5** gets reduced to **9**). It is evident that at these potentials, C−O bond cleavage via **8**, the reduction-first pathway, is much more likely than via the protonation-first pathway because **8** is much more stable than **6**. Generation of **8** is predicted to occur via **9** because its proton affinity is much higher than that of **5**. In summary, we find that driving the reaction forward to the CO_2-bound species is possible, even for the Mn catalyst, either with relatively strong Brønsted acids, a sufficiently negative applied potential, or a combination of both.

Activation Barriers. Next we analyze the effect of the different types of Brønsted acids on the activation free energies for C−O bond cleavage, the rate-limiting step during catalytic turnover. This will, together with the stability of CO_2 binding discussed above, determine the overall turnover rates. C−O bond cleavage is facilitated by a nearby proton donor, which can compensate the negative charge from the departing OH^- group and provide a proton to produce H_2O. We calculated the activation free energies for this process via the protonation-first and reduction-first pathways using phenol, TFE, MeOH, and H_2O. Because we are also interested in C−O bond cleavage without added Brønsted acid, we also consider the possibilities that the catalyst strips a proton from the MeCN solvent,[41] or from the electrolyte TBA via Hofmann degradation[42] (MeCN and TBA have computed pK_as of 36.4 and 7.9). TBA is particularly interesting because it has a low pK_a.

All computed activation barriers are summarized in Table 5. Two different trends are immediately evident. The barriers for

Table 5. Activation Barriers (kcal/mol) for C−O Bond Cleavage of Neutral and Reduced $[Mn(bpy)(CO)_3COOH]^{0/-}$ (6-Mn and 8-Mn) and $[Re(bpy)(CO)_3COOH]^{0/-}$ (6-Re and 8-Re)[a]

	ΔG‡ (Mn catalyst)		ΔG‡ (Re catalyst)	
Brønsted acid	**6** → **7**	**8** → **2**	**6** → **7**	**8** → **2**-CO
phenol	11.9	11.9	11.9	11.6
TFE	12.7	10.8	12.2	10.3
MeOH	18.3	15.0	17.5	13.7
H_2O	16.7	14.5	18.2	15.7
MeCN	26.3	22.8	28.8	24.6
TBA	40.3	34.7	37.5	35.5

[a]All values are given at the DFT-B3LYP level for standard states at room temperature.

the reduction-first pathway (**8** → **2**) are generally lower than the barriers for the protonation-first pathway (**6** → **7**). This is probably related to the negative charge of **8** compared with neutral **6**, as protonation of the negatively charged species

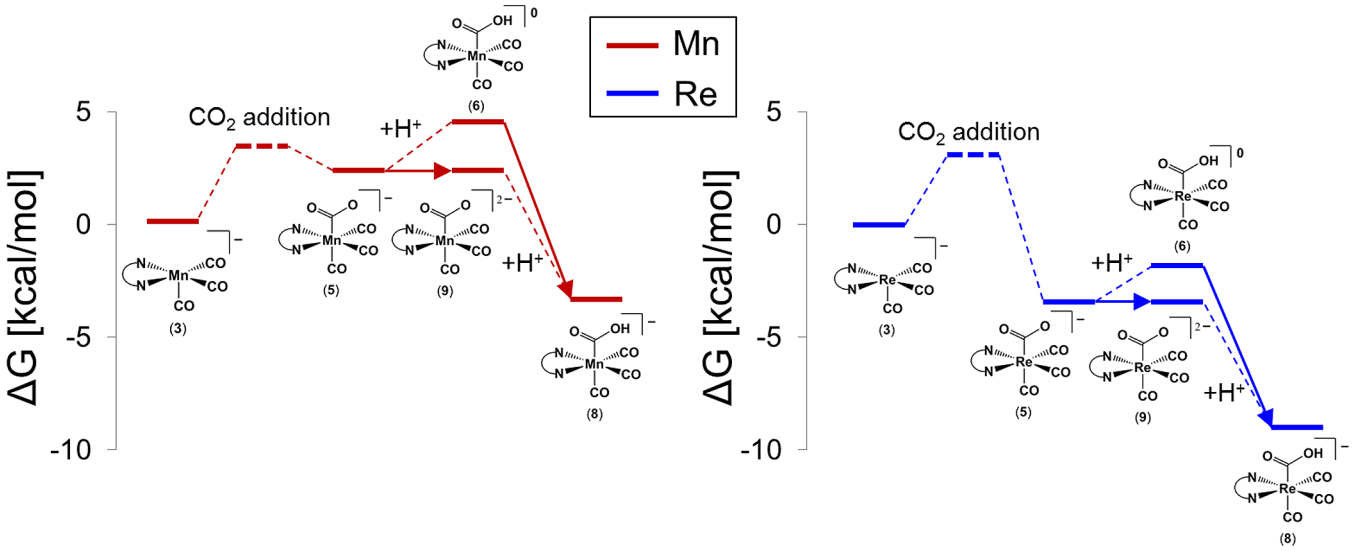

Figure 3. Free energy changes during the catalytic cycle reaction steps before C−O bond cleavage for the Mn and Re catalysts, using H_2O as the Brønsted acid. Reaction intermediates are depicted with solid lines and transition states with dashed lines. Arrows indicate electron transfer steps. The mechanisms are calculated at the least negative operating potentials for **5** → **9** (−2.03 and −1.87 V vs SCE for Mn and Re, respectively).

DOI: 10.1021/cs501687n
ACS Catal. 2015, 5, 900−908

should be more favorable and lower the TS energy. The more important trend is that barriers for the Re catalyst are mostly slightly lower than for the Mn catalyst. The only exception is H_2O, where the Re catalyst barriers are higher than for the Mn catalyst. This exception can be understood by examining the TS electronic structure.

In the TS geometries, as can be seen in SI Figure S1, the sixth ligand COOH is split into two fragments, OH and CO. The OH fragment is in an intermediate position between the CO ligand and the cosubstrate H_2O and already is partially bound to the H_2O Brønsted acid. Mulliken charge population analysis of the TS structures indicates that the H_2O−OH fragment has a charge population of about −0.85. The bpy ligand of the Mn catalyst carries 0.3 to 0.5 more positive charge population than the bpy ligand of the Re catalyst (respectively, 0.22 vs −0.11 in the **8** → **2** TS structure and 1.33 vs 0.81 in the **6** → **7** TS structure). The higher positive charge of the Mn bpy ligand electrostatically stabilizes the negatively charged H_2O−OH fragment more than the less positively charged Re bpy ligand, resulting in a decrease of the barrier heights in the case of H_2O as the proton donor. This effect is less important for the other Brønsted acids because they are much larger in size and are therefore interacting with the bpy ligand primarily via dispersion interactions (as found by visual inspection and can be seen from Figure S2). The activation barriers using MeCN as the proton donor are more than 8 kcal/mol higher than the other barriers, which is not surprising given its very low acidity. This should result in TOFs that are more than six orders of magnitude lower than the lowest TOFs with a Brønsted acid. TBA as a proton donor, despite having a favorable pK_a, shows activation barriers that are far too high, due to concomitant cleavage of both C−H and C−N bonds during the accompanying Hofmann degradation. Compared with H_2O, the barriers are at least 20 kcal/mol too high, resulting in TOFs that would be nine orders of magnitude lower than with MeCN. TBA will thus not be discussed further in the following.

Microkinetics Simulation. We saw that CO_2 binding, which ultimately influences the turnover rates, can be stabilized by stronger Brønsted acids as well by more negative applied potentials. Secondly, we computed the activation barriers of the rate-limiting step, which is the other determining factor for turnover rates. To analyze the effect of these different factors, we now perform microkinetics simulations on the catalytic cycle using a Matlab script that we already applied in ref 25. Here, we use a more advanced version of this microkinetics script, which explicitly incorporates the Brønsted acid/base pairs as well as MeCN as a proton donor into the reaction free energies of the protonation steps (eq 1). In addition, because protonation is not necessarily thermodynamically highly favorable anymore, backward reactions for the protonation reactions are also included. We use all the computed reaction free energies, reduction potentials, and activation free energies discussed above and simulate the reaction course at different applied potentials using the four Brønsted acids and MeCN as proton donors. This will reveal how pK_a and applied potential influence the TOFs and distribution of intermediates. As described in the Methods section, a shift of 2.65 kcal/mol (Re) and 4.7 kcal/mol (Mn) is applied to the DFT-B3LYP activation barriers for the C−O bond cleavage steps.

The predicted TOFs are depicted in Figure 4 together with available experimental TOFs. For the Re catalyst, the computed TOFs underestimate the experimental values by about one order of magnitude (similar to our findings in ref 25), with the

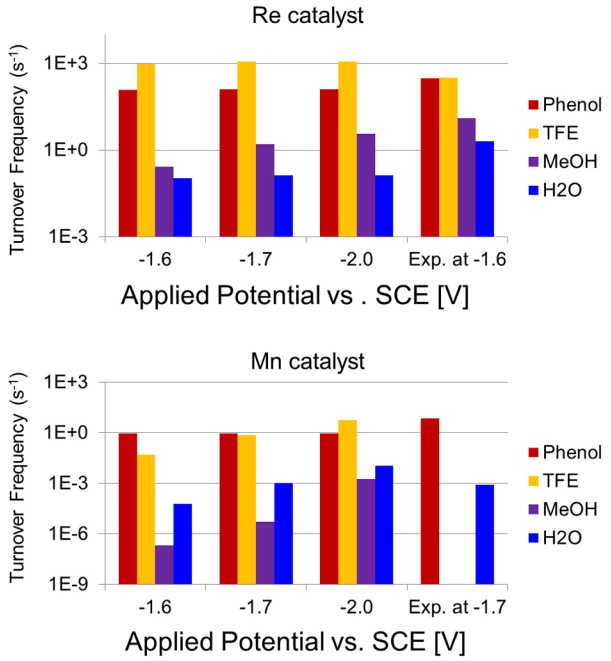

Figure 4. Computed TOFs at steady state for the Mn and Re catalysts under different reaction conditions. MeCN has much lower TOFs, which are not shown in order to better visualize the other TOFs. At −2.0 V vs SCE, MeCN has TOFs of 10^{-7} and 10^{-10} s^{-1} for the Re and Mn catalyst, respectively (the TOFs at −1.6 and −1.7 V vs SCE are below numerical accuracy). Experimental TOFs for the Re catalyst are computed from I_p/I_p° values taken from ref 16 using the approach described in the SI of ref 25 (TOFs for phenol, 304 s^{-1}; TFE, 312 s^{-1}; MeOH, 13 s^{-1}; H_2O, 2 s^{-1}). The experimental TOF for the Mn catalyst with phenol is taken from ref 25; the TOF for the Mn catalyst with H_2O is computed from data (turnover number, reaction time) taken from ref 28 (TOF for phenol, 7.2 s^{-1}; H_2O, 8×10^{-4} s^{-1}). The experimental data for Re and Mn were measured at an applied potential of −1.6 and −1.7 V vs SCE, respectively.

exception of TFE, which overestimates the experimental value by a factor of 3. (Note that an error of ∼1.3 kcal/mol in activation barrier produces an error of one order of magnitude in reaction rate at room temperature.) More importantly, the trend of the computed reaction rates is in agreement with the trend of the experimental TOFs, TFE > phenol > MeOH > H_2O. For the Mn catalyst, the only available experimental TOFs are for H_2O and phenol as proton donors. The computed and experimental values differ by less than one order of magnitude for both acids.

As seen in Figure 4, the TOFs of very weak acids are dependent on the applied potential. For the Mn catalyst, the TOF using phenol is independent of the applied potential, whereas TOFs with the other acids change significantly with potential. This dependence again reflects the endergonicity of CO_2 binding to the Mn catalyst. The effect is much less pronounced for the Re catalyst. For the Re catalyst, only MeOH shows increased TOF with potential (increases by a factor of 2 when increasing the potential from −1.7 to −2.0 V vs SCE). Wong et al. point out that when using MeOH and H_2O as acids, the Re catalyst achieves maximum activity at much higher acid concentrations than when using TFE and phenol.[16] To test this dependence, we repeated the microkinetics simulations at higher acid concentrations at −1.6 V vs SCE applied potential. Increasing the acid concentration only had an effect for MeOH. At 7.2 M MeOH (corresponding to

DOI: 10.1021/cs501687n
ACS Catal. 2015, 5, 900−908

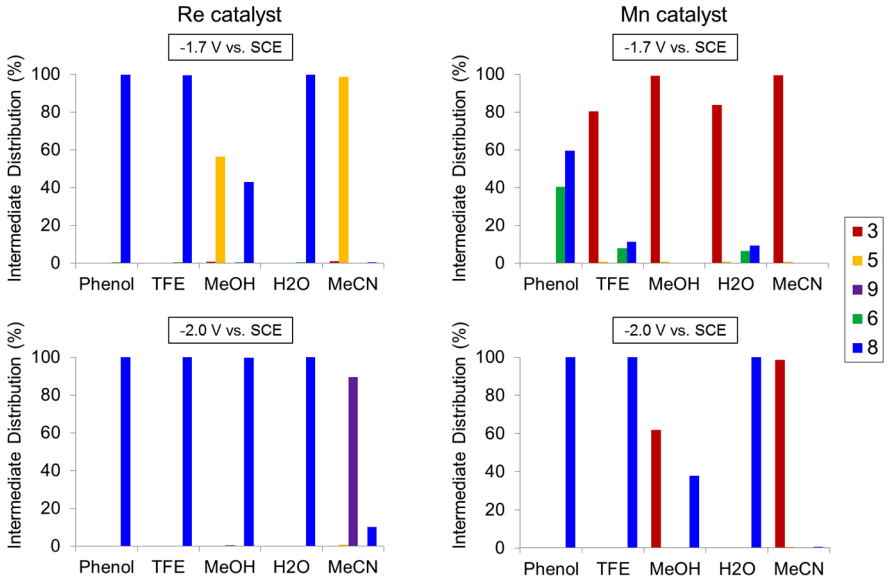

Figure 5. Intermediate distributions at steady state for the Mn and Re catalysts under different reaction conditions. Only intermediates **3**, **5**, **6**, **8**, and **9** accumulate in significant concentrations and are shown.

the reported concentration at which MeOH showed maximum activity,[16] compared to 0.57 M before), the computed TOF increased by a factor of 40, compared to a factor of 15 for the experimental values.

As already discussed for the activation barriers, a different trend exists for both catalysts when using H_2O as the Brønsted acid. The computed TOFs of the Re catalyst show the ordering TFE > phenol > MeOH > H_2O, while the computed TOFs for the Mn catalyst show a different ordering, TFE > phenol > H_2O > MeOH. This trend is similar to the trend found by Smieja et al. for the experimental rate constants when investigating the Re and Mn catalysts with *t*Bu-substituted bpy ligands.[18] The authors report that rate constants of the Re catalyst decrease in the order TFE > MeOH > H_2O (410, 94, and 5.7 s^{-1}), whereas the trend is TFE > MeOH ≈ H_2O (340, 130, and 120 s^{-1}) for the Mn catalyst.

The electrocatalytic reduction of CO_2 in the absence of Brønsted acids is modeled assuming that MeCN acts as a proton donor, providing one of its methyl hydrogens for protonation of CO_2 (**5** → **6** or **9** → **8**) and for C−O bond cleavage (**6** → **7** or **8** → **2**). At −1.7 V vs SCE, no turnover can be measured for this scenario. At −2.0 V vs SCE, a very slow catalytic turnover takes place, 1×10^{-7} s^{-1} for the Re catalyst and 1×10^{-10} s^{-1} for the Mn catalyst. Experimentally, Smieja et al. report, for a Mn catalyst with *t*Bu-substituted bpy ligands, no measurable catalytic turnover in the absence of Brønsted acids.[18] However, for the respective Re catalyst, under the same reaction conditions, they measure an experimental TOF that is only one order of magnitude slower than with H_2O. Our model cannot fully explain the experimental results. Our simulations indicate that the Re catalyst with MeCN as proton donor can catalyze CO_2 reduction only at a TOF six orders of magnitude slower compared to the TOF with added H_2O, a difference of five orders of magnitude compared to the experimental trend. This means that MeCN alone cannot be responsible for catalytic turnover observed with the Re catalyst. We will discuss further possibilities below.

Because we found reasonable agreement between our model and experimental results, next we investigate further the catalytic turnover and make predictions for catalytic pathways and intermediate distributions at varying applied potentials and using no or varying Brønsted acids. Figure 5 displays the intermediate distributions for both catalysts at −1.7 and −2.0 V vs SCE. For the Re catalyst, at both potentials, only **8** (not **6**) accumulates. The reduction-first pathway is always taken (as already discussed in ref 25). At −1.7 V vs SCE, the acids phenol, TFE, and H_2O all lead to protonation of the CO_2 adduct and further reduction to yield **8**. Note that H_2O is among this group of stronger acids only because of its acidification in the presence of CO_2 (vide supra). With the very weak acid MeOH, the unprotonated CO_2 adduct **5** is slightly more stable than **8**, and because of the low exoergicity of **3** → **5**, there is also a tiny fraction of **3** present. Switching the potential to −2.0 vs SCE strongly shifts the equilibrium for MeOH towards **8**, allowing a larger catalytic turnover (which is reflected in the TOF, vide supra). We discussed above that for MeOH, not only the applied potential but also the acid concentration can change the turnover rate. Thus we can ask how does the intermediate distribution change when the MeOH concentration is increased (as above, from 0.57 to 7.2 M, and at an applied potential of −1.6 V vs SCE)? Our microkinetics simulations show that the higher acid concentration drives protonation forward, increasing the relative concentration of **8** (7% to 23%) at the expense of **5** (90% to 72%). This increase in available reactant for C−O bond cleavage results in the 40-fold increase in computed TOF mentioned earlier. And why do the TOFs for the other acids not change when increasing acid concentration? In those cases, the relative ratio of **8** is almost at 100%, and this cannot be increased substantially by increasing the acid concentration or applying a more negative potential.

The simulations for the Re catalyst without added Brønsted acid, that is, with MeCN as proton donor, show very different results compared to the simulations with Brønsted acid. At −1.7 V vs SCE, **5** is most stable, and **8** is accumulating at less than 0.1%. Switching the potential to −2.0 V vs SCE has a large effect because the strong negative potential reduces all CO_2 adducts **5** to **9**, and the acidity of MeCN is strong enough to protonate 10% of this population to yield **8**. A small, but significant, amount of **8** is now available to react further and

DOI: 10.1021/cs501687n
ACS Catal. 2015, 5, 900−908

cleave the C−O bond. As discussed above, however, the reaction rate with MeCN is too low because the activation barrier for C−O bond cleavage with MeCN as the proton donor is much too high. However, if trace amounts of another species are present that can lead to C−O bond cleavage, the reaction could proceed from this point. For example, since one molecule of H_2O is produced per C−O bond cleavage step, this molecule can potentially act as the Brønsted acid for the C−O bond cleavage in the next cycle. However, if MeCN provides the protons to protonate CO_2 (**9** + H_3CCN ↔ **8** + H_2CCN^-), one could argue that every H_2O that is produced immediately gets deprotonated by H_2CCN^- (pK_a of MeCN, 36.4; pK_a of H_2O in the presence of CO_2, 26.6). Thus it remains unclear as to how the Re catalyzed reaction proceeds in the absence of a proton donor other than MeCN.

For the Mn catalyst, the intermediate distribution looks quite different at −1.7 V vs SCE. For phenol, CO_2 binding to the catalyst can be driven forward completely, despite the endergonicity of **3** → **5**. For all other acids considered, CO_2 binding is too unfavorable, and **3** accumulates instead to more than 70% (73%, 80.3%, and 99.1% for H_2O, TFE, and MeOH, respectively). Depending on the pK_a of the Brønsted acid, **6** and **8** can accumulate to some extent (the distribution of **6** and **8** sums up to 26.5%, 19.1%, and 0.2% for H_2O, TFE, and MeOH, respectively). For all acids, however, the ratio between **6** and **8** is about 2:3, determined by the applied potential and the reduction potential of **6**, that is, both reduction-first and protonation-first pathways are taken at this potential, independent of the Brønsted acid used. Switching the potential to −2.0 V vs SCE increases the stabilities of the CO_2-bound species **9** and **8**. Only MeOH and MeCN still show a significant amount of **3**. For phenol, TFE, and H_2O, **8** is now accumulating at 100%, and changing the applied potential to more negative potentials will not further affect their TOFs. With MeCN as proton donor, a small fraction of 0.5% of **8** accumulates at this potential. This small amount of **8**, about two orders of magnitude less than for the Re catalyst at similar conditions, is available for C−O bond cleavage. This translates to the much lower computed TOF (vide supra).

CONCLUSIONS

We have performed a computational investigation of electrocatalytic CO_2 reduction by Mn(bpy)$(CO)_3$Br (**1-Mn**) and Re(bpy)$(CO)_3$Cl (**1-Re**) without added Brønsted acid as well as with four different Brønsted acids (phenol, TFE, MeOH, and H_2O) and directly compared their catalytic mechanisms. Experimentally, the TOFs vary when using different Brønsted acids. In addition, for the same Brønsted acid, the TOFs are lower for the Mn catalyst compared to the Re catalyst. Our computed TOFs reproduce the available experimental trends and deviate from the experimental TOFs by about one order of magnitude. Mn and Re catalysts, each with a *t*Bu-disubstituted bpy ligand, exhibit differing trends in measured TOFs (TOFs for the Re catalysts: TFE > MeOH > H_2O, and for the Mn catalysts: TFE > MeOH ≈ H_2O). Our computations for the catalysts with an unsubstituted bpy ligand largely reproduce this trend. Analyzing the electronic structure of the TS structures shows that the bpy ligand of the Mn catalyst exhibits a charge about 0.3 to 0.5 more positive than the bpy ligand of the Re catalyst. The more positive charge of the Mn bpy ligand stabilizes the TS structure for the C−O bond cleavage step with H_2O as the Brønsted acid, changing the trend in TOFs observed. This property of the Mn bpy ligand could potentially be used for other small cosubstrate acids to increase rates. Alternatively, different bpy ligand substituents could mimic this effect for both catalysts.

The ratio of the C−O bond cleavage reactants (**6** and **8**) compared to their precursors (**3**, **5**, and **9**) strongly influences the observed TOF. For very weak acids, these precursors accumulate to a significant extent. Increasing the applied potential or increasing the concentration of acid drives the protonation of these precursors forward and thus increases the TOF. Overall, for very weak acids, we found that the turnover rate is not at its maximum and is strongly dependent on the applied potential and the acid concentration.

It was reported that the Mn catalyst does need the addition of Brønsted acids for catalytic turnover, whereas the Re catalyst operates without added Brønsted acid. As a means to investigate this, we used the solvent MeCN and the electrolyte TBA as proton donors for our calculations. At an applied potential of −2.0 V vs SCE, we found that MeCN protonates the CO_2-bound complex to an extent of ∼10% (Re) and 0.5% (Mn). This means that MeCN can help accumulate **8**, the reactant for the C−O bond cleavage step, significantly more in the case of the Re catalyst compared to the Mn catalyst. However, the activation barrier for C−O bond cleavage with MeCN is much too high, and thus, the predicted TOF for the Re catalyst is much too low compared with the experimental value. The activation barrier for C−O bond cleavage with TBA is even higher than with MeCN, which also rules out Hofmann degradation as the direct source for protonation. We thus conclude that either trace amounts of other proton sources or produced H_2O during catalytic turnover are assisting in C−O bond cleavage in this case, or that a mechanism similar to the outer sphere reduction as described by Saveant et al. is responsible for CO production.[43] In this mechanism, two radical CO_2 anions couple to form oxalate, which then decomposes to CO and carbonate. This mechanism can be checked experimentally because equimolar amounts of CO and carbonate are produced.

ASSOCIATED CONTENT

Supporting Information

The following file is available free of charge on the ACS Publications website at DOI: 10.1021/cs501687n.

Information on the applied potential/pK_a relation, pK_as for explicitly solvated Brønsted acids, the TS geometry for C−O bond cleavage with H_2O, atomic coordinates of all optimized molecules, and the total dispersion correction for all TS geometries (PDF)

AUTHOR INFORMATION

Corresponding Author

*E-mail: eac@princeton.edu.

Notes

The authors declare no competing financial interest.

ACKNOWLEDGMENTS

We thank Andrew M. Ritzmann for providing the initial version of the microkinetics script and for helpful discussions. This work was supported by the Air Force Office of Scientific Research through the MURI program (AFOSR Award No. FA9550-10-1-0572).

DOI: 10.1021/cs501687n
ACS Catal. 2015, 5, 900−908

REFERENCES

(1) Inglis, J. L.; MacLean, B. J.; Pryce, M. T.; Vos, J. G. *Coord. Chem. Rev.* **2012**, *256*, 2571−2600.
(2) Kuhl, K. P.; Cave, E. R.; Abram, D. N.; Jaramillo, T. F. *Energy Environ. Sci.* **2012**, *5*, 7050−7059.
(3) Benson, E. E.; Kubiak, C. P.; Sathrum, A. J.; Smieja, J. M. *Chem. Soc. Rev.* **2009**, *38*, 89−99.
(4) Kumar, B.; Llorente, M.; Froehlich, J.; Dang, T.; Sathrum, A.; Kubiak, C. P. *Annu. Rev. Phys. Chem.* **2012**, *63*, 541−569.
(5) Hori, Y., Electrochemical CO2 Reduction on Metal Electrodes. In *Modern Aspects of Electrochemistry*, Vayenas, C.; White, R.; Gamboa-Aldeco, M., Eds. Springer: New York, 2008; Vol. *42*, pp 89−189.
(6) Qiao, J.; Liu, Y.; Hong, F.; Zhang, J. *Chem. Soc. Rev.* **2014**, *43*, 631−675.
(7) Windle, C. D.; Perutz, R. N. *Coord. Chem. Rev.* **2012**, *256*, 2562−2570.
(8) Costentin, C.; Robert, M.; Saveant, J.-M. *Chem. Soc. Rev.* **2013**, *42*, 2423−2436.
(9) Kondratenko, E. V.; Mul, G.; Baltrusaitis, J.; Larrazabal, G. O.; Perez-Ramirez, J. *Energy Environ. Sci.* **2013**, *6*, 3112−3135.
(10) Appel, A. M.; Bercaw, J. E.; Bocarsly, A. B.; Dobbek, H.; DuBois, D. L.; Dupuis, M.; Ferry, J. G.; Fujita, E.; Hille, R.; Kenis, P. J. A.; Kerfeld, C. A.; Morris, R. H.; Peden, C. H. F.; Portis, A. R.; Ragsdale, S. W.; Rauchfuss, T. B.; Reek, J. N. H.; Seefeldt, L. C.; Thauer, R. K.; Waldrop, G. L. *Chem. Rev.* **2013**, *113*, 6621−6658.
(11) Grice, K. A.; Kubiak, C. P., Chapter Five - Recent Studies of Rhenium and Manganese Bipyridine Carbonyl Catalysts for the Electrochemical Reduction of CO2. In *Adv. Inorg. Chem.*, Michele, A.; Rudi van, E., Eds. Academic Press: 2014; Vol. *66*, pp 163−188.
(12) Froehlich, J. D.; Kubiak, C. P. *Inorg. Chem.* **2012**, *51*, 3932−3934.
(13) Smieja, J. M.; Kubiak, C. P. *Inorg. Chem.* **2010**, *49*, 9283−9289.
(14) Smieja, J. M.; Benson, E. E.; Kumar, B.; Grice, K. A.; Seu, C. S.; Miller, A. J. M.; Mayer, J. M.; Kubiak, C. P. *Proc. Natl. Acad. Sci. U.S.A.* **2012**, *109*, 15646−15650.
(15) Hawecker, J.; Lehn, J. M.; Ziessel, R. *J. Chem. Soc., Chem. Commun.* **1984**, 328−330.
(16) Wong, K.-Y.; Chung, W.-H.; Lau, C.-P. *J. Electroanal. Chem.* **1998**, *453*, 161−169.
(17) Benson, E. E.; Kubiak, C. P. *Chem. Commun.* **2012**, *48*, 7374−7376.
(18) Smieja, J. M.; Sampson, M. D.; Grice, K. A.; Benson, E. E.; Froehlich, J. D.; Kubiak, C. P. *Inorg. Chem.* **2013**, *52*, 2484−2491.
(19) Grice, K. A.; Gu, N. X.; Sampson, M. D.; Kubiak, C. P. *Dalton Trans.* **2013**, *42*, 8498−8503.
(20) Keith, J. A.; Grice, K. A.; Kubiak, C. P.; Carter, E. A. *J. Am. Chem. Soc.* **2013**, *135*, 15823−15829.
(21) Machan, C. W.; Sampson, M. D.; Chabolla, S. A.; Dang, T.; Kubiak, C. P. *Organometallics* **2014**, *33*, 4550−4559.
(22) Sampson, M. D.; Froehlich, J. D.; Smieja, J. M.; Benson, E. E.; Sharp, I. D.; Kubiak, C. P. *Energy Environ. Sci.* **2013**, *6*, 3748−3755.
(23) Johnson, F. P. A.; George, M. W.; Hartl, F.; Turner, J. J. *Organometallics* **1996**, *15*, 3374−3387.
(24) Benson, E. E.; Sampson, M. D.; Grice, K. A.; Smieja, J. M.; Froehlich, J. D.; Friebel, D.; Keith, J. A.; Carter, E. A.; Nilsson, A.; Kubiak, C. P. *Angew. Chem., Int. Ed.* **2013**, *52*, 4841−4844.
(25) Riplinger, C.; Sampson, M. D.; Ritzmann, A. M.; Kubiak, C. P.; Carter, E. A. *J. Am. Chem. Soc.* **2014**, *136*, 16285−16298.
(26) Agarwal, J.; Sanders, B. C.; Fujita, E.; Schaefer Iii, H. F.; Harrop, T. C.; Muckerman, J. T. *Chem. Commun.* **2012**, *48*, 6797−6799.
(27) Morris, A. J.; Meyer, G. J.; Fujita, E. *Acc. Chem. Res.* **2009**, *42*, 1983−1994.
(28) Bourrez, M.; Molton, F.; Chardon-Noblat, S.; Deronzier, A. *Angew. Chem., Int. Ed.* **2011**, *50*, 9903−9906.
(29) Neese, F. *Wiley Interdiscipl. Rev. - Comput. Mol. Sci.* **2012**, *2*, 73−78.
(30) Klamt, A.; Schürmann, G. *J. Chem. Soc. Perk. T. 2* **1993**, *1993*, 799−805.
(31) Zheng, J.; Xu, X.; Truhlar, D. *Theor. Chem. Acc.* **2011**, *128*, 295−305.
(32) Kelly, C. P.; Cramer, C. J.; Truhlar, D. G. *J. Phys. Chem. B* **2006**, *111*, 408−422.
(33) Becke, A. D. *Phys. Rev. A* **1988**, *38*, 3098−3100.
(34) Becke, A. D. *J. Chem. Phys.* **1993**, *98*, 5648−5652.
(35) Lee, C.; Yang, W.; Parr, R. G. *Phys. Rev. B* **1988**, *37*, 785−789.
(36) Grimme, S.; Antony, J.; Ehrlich, S.; Krieg, H. *J. Chem. Phys.* **2010**, *132*, 154104.
(37) Hansen, A.; Liakos, D. G.; Neese, F. *J. Chem. Phys.* **2011**, *135*, 214102.
(38) Fawcett, W. R. *Liquids, Solutions, and Interfaces: From Classical Macroscopic Descriptions to Modern Microscopic Details*. Oxford University Press: 2004.
(39) Fernández-Ramos, A.; Miller, J. A.; Klippenstein, S. J.; Truhlar, D. G. *Chem. Rev.* **2006**, *106*, 4518−4584.
(40) Fujita, E.; Creutz, C.; Sutin, N.; Szalda, D. J. *J. Am. Chem. Soc.* **1991**, *113*, 343−353.
(41) Slater, S.; Wagenknecht, J. H. *J. Am. Chem. Soc.* **1984**, *106*, 5367−5368.
(42) Bolinger, C. M.; Sullivan, B. P.; Conrad, D.; Gilbert, J. A.; Story, N.; Meyer, T. J. *J. Chem. Soc., Chem. Commun.* **1985**, 796−797.
(43) Gennaro, A.; Isse, A. A.; Severin, M.-G.; Vianello, E.; Bhugun, I.; Saveant, J.-M. *J. Chem. Soc., Faraday Trans.* **1996**, *92*, 3963−3968.

DOI: 10.1021/cs501687n
ACS Catal. 2015, 5, 900−908